Processing and Application of Ceramics 8 [2] (2014) 93–99
DOI: 10.2298/PAC1402093R

Effect of primary particle size on spray formation, morphology and internal structure of alumina granules and elucidation of flowability and compaction behaviour

Pandu Ramavath, Ramanathan Papitha, Malotha Ramesh, Pitchuka Suresh Babu, Roy Johnson*

Centre for Ceramic Processing, International Advanced Research Centre for Powder Metallurgy and New Materials, Hyderabad-500005, India

Received 12 May 2014; Received in revised form 6 June 2014; Accepted 12 June 2014

Abstract

Three different alumina powders with varying particle sizes were subjected to spray drying under identical conditions and effect of particle size on heat transfer efficiency and mechanism of formation of granules was elucidated. Morphology, internal structure and size distribution of granules were studied and evaluated with respect to their flow behaviour. In order to estimate the elastic interaction of granules, the granules were subjected to compaction under progressive loading followed by periodic unloading. Compaction curves were plotted and compressibility factor was estimated and correlated with predicted and measured green density values.

Keywords: *alumina powders, spray drying, pressing, structural characterization, modelling*

I. Introduction

Spray drying is one of the widely used unit operations and effective single step drying and granulation technique initially used extensively by the dairy industry [1–5]. This technology extends now into various vital industrial sectors i.e. pharmaceuticals, food, agrochemicals, heavy and fine chemicals, detergents, metallurgical and ceramic industries [6–14]. Several methods of drying such as drying laboratory ovens, rotary evaporators, freeze dryers etc. produce particles of irregular shapes and sizes [14]. Spray drying involves atomization of a precursor fluid into droplets with high surface to mass ratio, which are than exposed to the hot air medium in a drying chamber. Direct contact with the heated air causes effective heat transfer, instantaneous evaporation of the solvent and uniform transformation of the fluid into dry granules in the one step process [15,16].

Today powder manufacturing industries are looking for high powder quality along with high productivity, lower cost and minimal environmental impact. Due to the inherent flexibility in operation and modification of process parameters of spray drying, it is possible to engineer the powder properties to the predefined specifications, such as granule size, morphology, density and also the moisture content. Efficiency of the spray drying process is a strong function of momentum, heat and mass transfer to the droplets and corresponding material, energy balance and droplet drying kinetics [17].

Compaction of ceramics is one of the common industrial forming processes and quality of the formed compact is a strong function of granules' properties with optimum morphology [18–20]. This is due to the fact that the surface forces (Van der Waals) on these particles will spontaneously tend to form low density aggregates. These aggregates result in inhomogeneous die filling and non-consistent compacted parts. Granulation by spray drying facilitates the addition of organic additives which weakly bounds the primary particles and ensure good deformability under compaction pressure. Additionally, the binders also impart strength of the compacted green parts [22,23]. Rearrangement of granules under compaction stresses depends mainly on granule packing structure, granule size distribution and hardness. Granules with high flowability and less intergran-

*Corresponding author: tel: +91 402 444 3169
fax: +91 402 444 2699, e-mail: *royjohnson@arci.res.in*

ular friction facilitate better compact quality with lesser packing faults [23–27]. Though spray drying is widely practiced, challenges with users are to achieve consistent quality of the granules. Hence, it is mandatory to understand the process and the effects of various parameters on the quality and productivity.

The main objective of the present study is to evaluate the effect of primary particle size of alumina powder on the morphology and internal structure of spray dried granules and to correlate the granule properties with respect to flowability. Further, the compaction behaviour of the granules was also studied through progressive loading and periodic unloading followed by plotting of compression curves and estimation of compressibility factor.

II. Experimental

Alumina powders of three grades MR-01, HIM-10 (Nalco, India) and SM-8 (Baikowski, France) of varying particle size were subjected to phase analysis by X-ray diffraction (Bruker AXS GmbH, Karlsruhe, Germany) and particle size measurement using laser diffraction technique (Nanosizer, Malvern). Morphology of the powders is also evaluated using scanning electron microscope (SE300/N, Hitachi, Japan). The alumina powders were dispersed in aqueous medium to form slurries having solid fraction of 30 wt.% using Darvan 821A (R.T. Vanderbilt Co., Inc., Norwalk, CT, USA) as a dispersant and 2 wt.% PVA as the binder. The suspension was then milled for 4 h in polypropylene bottles in a pot jar mill with 10 revolutions per minute using alumina grinding balls of 4 mm diameter at 1 : 1 charge to balls ratio to achieve expected solid loadings.

The slurries prepared as described above were subjected to spray drying using a laboratory spray dryer BUCHI-B-290/295 model. Typical spray drying parameters are shown in Table 1. Thermodynamic considerations on spray drying process can be defined through the relationships by applying a mass and energy balance [17]. For single pass mode using spray dryer the outlet temperature can be correlated with the equation:

$$T_{outlet} = T_{inlet} - \frac{M_{soln} \cdot (1 - X_{solid}) \cdot \Delta H_{vap}}{M_{gas} \cdot C_p} \qquad (1)$$

where M_{soln} and M_{gas} are the flow rate of the slurry and hot air, respectively, X_{solid} is the solid content in the slurry, C_p is the specific heat of the air, ΔH_{vap} is the heat of vaporization of the slurry and T_{inlet} is the inlet temperature of the hot air.

In order to evaluate the effect of spray drying parameters, the granules were subjected to SEM analysis for size, distribution and morphology of the granules. Further, the granule flow characteristics are analysed using the powder flow analyser (Stable Micro System, UK). Internal structure of green granules was also evaluated using SEM imaging of the granules after subjecting them to mounting and gentle polishing. Further, attempts were made to generate the compaction curves for different granule morphologies.

Compaction behaviour of MR-01, HIM-10 and SM-8 granules was evaluated by using a compaction die with 10 mm diameter placed between the platens of a universal testing machine (Instron, 4483). 1 g of the powder was used for compaction and load-displacement curves were recorded using a computer interface. Before carrying out the compaction process, the powder was compacted with initial pressure of 5 MPa, as it is difficult to record reliable measurements at pressures below 5 MPa. The displacement values of the top punch were recorded [23,24]. Powder was further compacted up to 260 MPa with defined increment of pressure and for every preset value of these pressures the displacements of the top punch from the initial position are recorded. When the compaction cycle for each pressure is completed, the true compaction of the powder body without contribution of the elastic interaction between the particles can be obtained from the plot of height versus pressure. Further on, the segments were extrapolated to the axis of ordinates at the attained level of the initial pressure (5 MPa). Height of the compact (H_i) at different compaction pressures was calculated based on the value of the h_k from the equation:

$$H_i = H_k + (h_k - h_{k-1}) \qquad (2)$$

where H_i is thickness of the compact under compaction processing, H_k is pellet thickness at maximum pressure, h_k is displacement at k^{th} value and h_{k-1} is displacement at $k{-}1^{th}$ values [24].

III. Results and discussion

XRD patterns of the powders MR-01, HIM-10 and SM-8, used in the present study, along with the particle size and morphology are shown in Figs. 1, 2 and 3, respectively. It is evident that all the powders have alumina as a major phase.

Table 1. Spray drying parameters

Operation parameter	MR-01	HIM-10	SM-8
Inlet temperature [°C]	210	210	210
Outlet temperature [°C] (measured)	112	108	119
Slurry feed rate [ml/min]	11	11	11
Hot air feed rate [m^3/h]	40	40	40
Atomization pressure [bar]	6	6	6

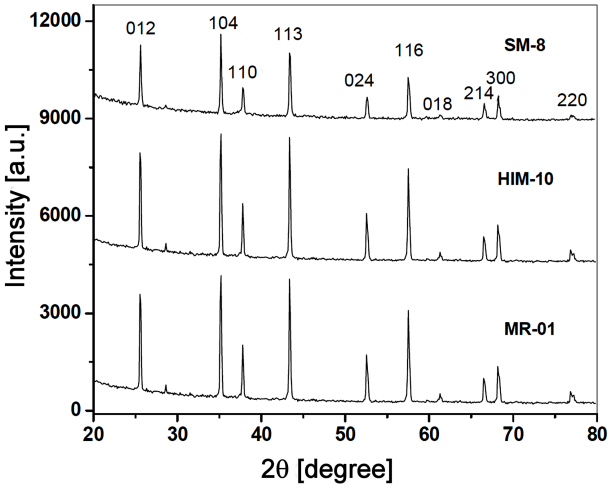

Figure 1. XRD patterns of alumina powders: MR-01, HIM-10, SM-8

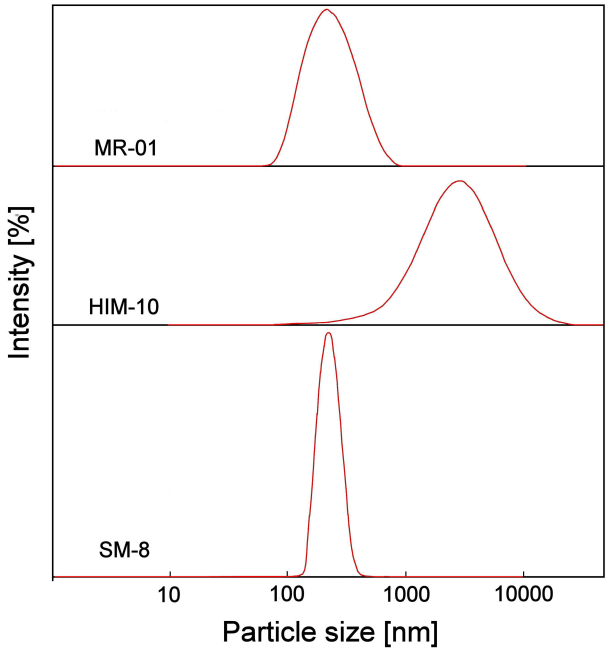

Figure 2. Particle size distribution of alumina powders: MR-01, HIM-10, SM-8

However, there is a large variation in particle sizes. The alumina powders MR-01, HIM-10 and SM-8 exhibit the particle size (D_{50}) of 0.8 μm, 6 μm and 0.25 μm, respectively. Morphologies of the powder MR-01 and HIM-10 are similar (particles have different geometric shapes, high aspect ratio and are agglomerated), but morphology of the powder SM-8 characterizes discrete particles with narrow size distribution and mostly equi-axed shape.

It is evident from the spray drying parameters depicted in Table 1 that there is a distinct difference in the outlet temperature which is a strong function of other contributing parameters, such as: inlet temperature, hot air flow rate and slurry feed rate, which were kept identical in all cases. The outlet temperature estimated by the equation (1) was around 111 °C. Heat input of the hot air should be equal to the sum of the heat output of the air (112 °C) and the temperature of spray dried granules and heat losses in the spray drier. The measured outlet air temperature for the sample MR-01 is close to the predicted values and granules exhibited a moisture content of 2% indicating the minimum heat losses in continuous operation. However, in case of the sample SM-8 the measured outlet air temperature (119 °C) exceeded the predicted values. Further, SM-8 granules exhibited a moisture content of >1%, whereas relatively high moisture content of 4% was observed for the sample HIM-10. In a dynamic system the heat transfer properties depend on several variables such as hot air velocity, particle size, size distribution, shape as well as the thermo-physical properties of the particles. Under the present experimental conditions, as the particle size is the major variable, the difference in moisture content could be correlated with the heat transfer effects on particle properties.

SEM micrographs of the spray dried granules MR-01, HIM-10 and SM-8 are shown in Fig. 4. During atomization of the slurry under air pressure, the granules get into direct contact with the hot air and the water starts evaporating from the surface and consequently the internal water get transported to the surface by capillary action. Further, the solids concentrate on the surface and droplet shrinks due to the inward movement

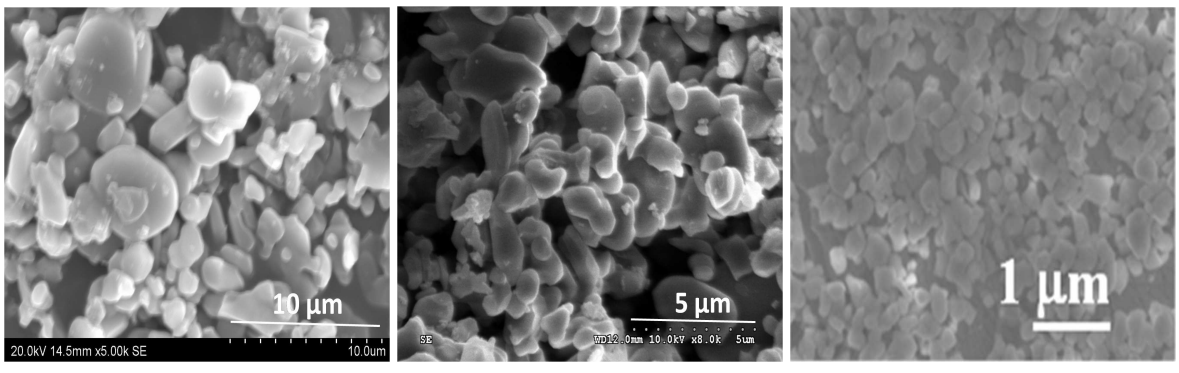

(a) (b) (c)

Figure 3. SEM micrographs of alumina powders: a) MR-01, b)HIM-10 and c) SM-8

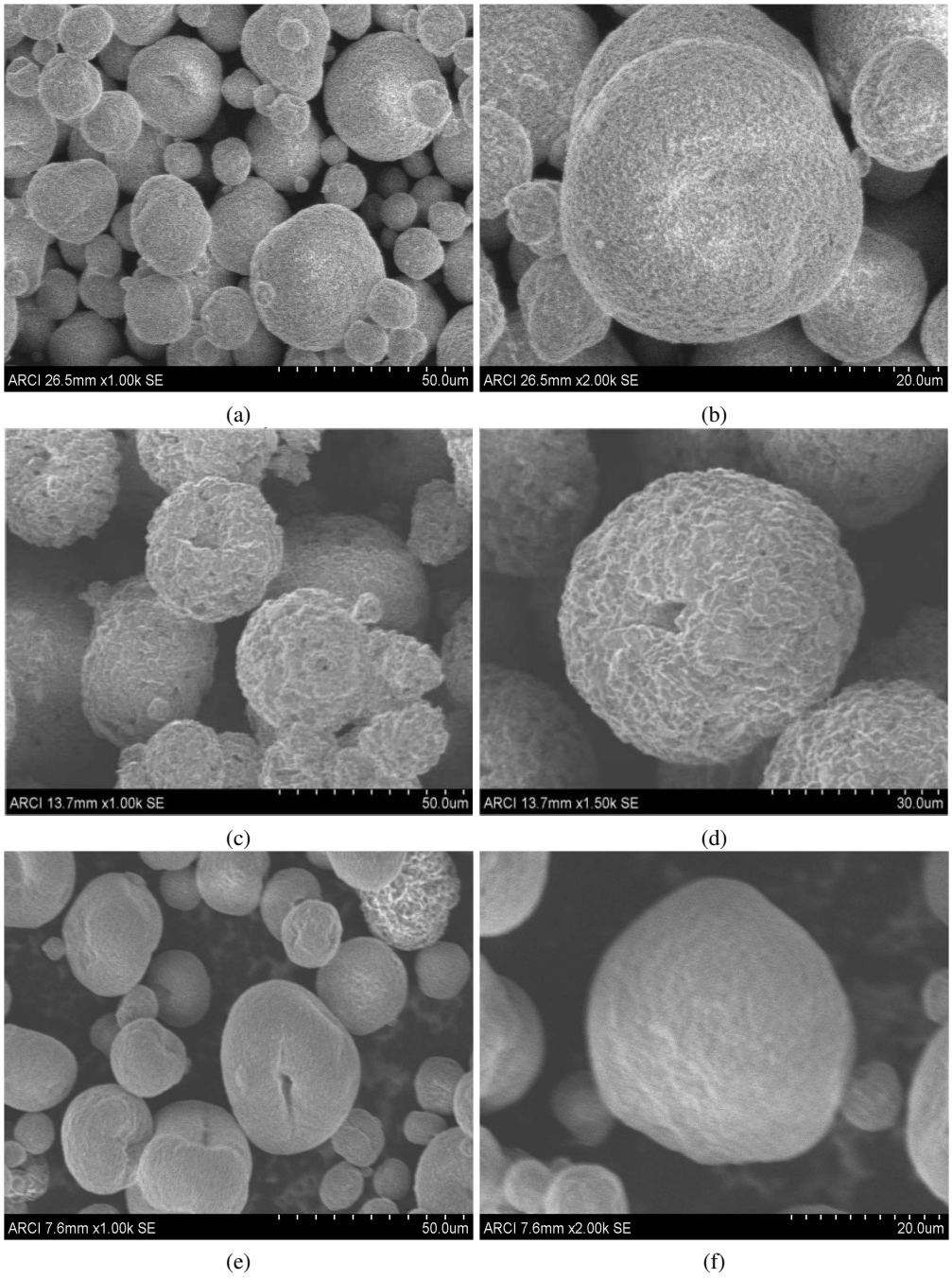

Figure 4. SEM micrographs of alumina granules: a,b) MR-01, c,d) HIM-10 and e,f) SM-8

of the boundaries. It is evident that MR-01 granules are relatively dense (Fig. 4a,b). Due to the fine sizes (D_{50} = 0.8 μm) the MR-01 droplet shrinks slowly leading to a uniform distribution of solids and formation of dense granules without significant crust formation. This is also evident from the internal structure of the granules depicted in Fig. 5a. It is well known that the high density granules are desired for compaction. However, too high density of granules can also be a disadvantage. Nevertheless surfaces are porous as they are the escape path of residual water vapour from inside of the granule after achieving the thermal equilibrium with the hot gas.

In the case of the sample SM-8, particle size is also fine (D_{50} = 0.25 μm) and it is expected to have a more uniform coating of organic binders on the surface of the particles dispersed in the slurry. The granules are mostly spherical along with a few doughnut shapes. During drying the organic binders along with the much finer particles are expected to form an elastic film, with binder reaching outer layer with very low permeability to the moisture (Fig. 5c). On achieving the thermal equilibrium with the hot air there will be evaporation inside the droplet causing ballooning (Fig. 5c). The migration of the binders along with the densely packed outer shell may resist fracture during compaction causing compaction defects.

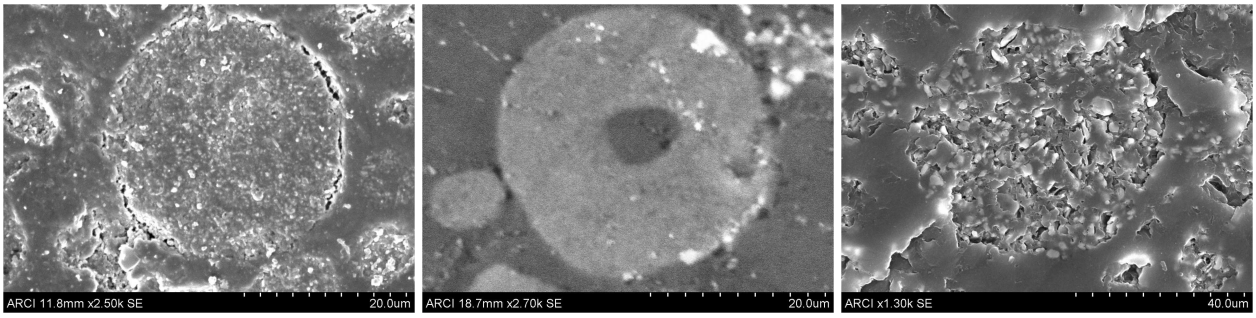

(a) (b) (c)

Figure 5. Internal structure of the granules of: a) MR-01, b) HIM-10 and c) SM-8

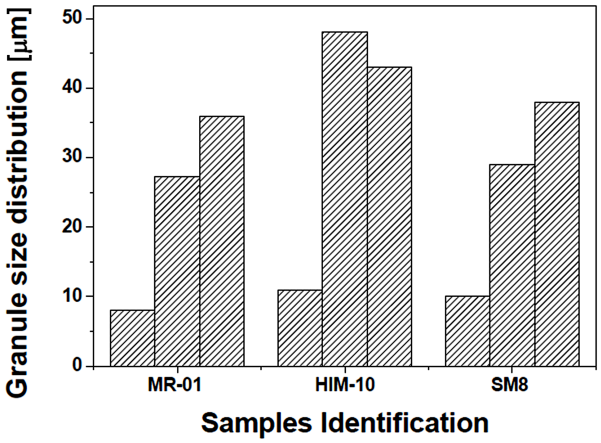

Figure 6. Granule size distribution of: MR-01, HIM-10 and SM-8 alumina

Unlike other samples, in the case of HIM-10 the granules are constituted of agglomerates with distinct voids on the surface. In this case, the droplets shrink faster leading to the thickening of the surface preventing the free escape of the water vapour due to the low permeability. During the thermal equilibrium with the hot air temperature exceeds the boiling point of water internal pressure build up and surface bursts forming the voids on the surface. The ground surface of the granules (Fig. 5b) reveals agglomerates with interconnected voids.

Apparent density and flow property of the granules are shown in Table 2. Apparent density values are found to correlate well with the observed microstructure. The dense granules exhibited an apparent density of 0.96 g/cm^3, 0.85 g/cm^3 and 0.63 g/cm^3 for the samples MR-01 SM8 and HIM-10, respectively. During the first stage of compaction process the density increases through granule rearrangement and pore reduction followed by granule deformation to about 80% of green density. Later, the compaction reaches the final stage the granule fracture and become a green compact with isolated pores (having 60% of theoretical density (%TD)). The stress induced by rearrangement and deformation of granules depends primarily on the flowability, packing of primary particles, granule size distribution and hardness. Granules with the high flowability and low intergranular friction are expected to have lesser packing flaws. Cohesion index measurement of the granules revealed relatively higher flowability for SM-8 sample. Though the apparent density of the sample SM-8 is lower than for MR-01 due to ballooning, the relatively higher flowability can be attributed to the hard skin which favours the free flow. HIM-10 on the other hand possess several surface voids (Fig. 5b) which restricts the flow while flowing against each other exhibiting comparatively poor flowability though with the cohesion index value of 9.58 (cohesion index <11, flowability categorization as described elsewhere [28]) corresponds to the free flowing behaviour. However, in general spray drying has substantially improved the flowability of all powders with different geometric shapes to a greater extent.

Granule size distribution of the samples MR-01, HIM-10 and SM-8 are shown in Fig. 6. Size of the granules formed during spray drying mainly depends on the size of the atomized droplet, solid loading of the slurry, particle size of the primary particles and feed rate of the slurry. Since all parameters, except the particle size, are maintained identical, the granule size distribution can be correlated to the primary particle size. Though the granule size distribution is found to be a function of the initial particle size in case of HIM-10 and MR-01, the granules size distributions are almost the same for MR-01 and SM-8 powders. This can be attributed to the fact that skin hardening and ballooning effect observed in the case of SM-8 does not allow shrinkage of the granules

Table 2. Spray drying parameters

Sample ID	Cohesion index, powders	Cohesion index, granules	Apparent density [g/cm^3]
MR-01	26	7.54	0.96
HIM-10	38	9.58	0.63
SM-8	15	6.7	0.85

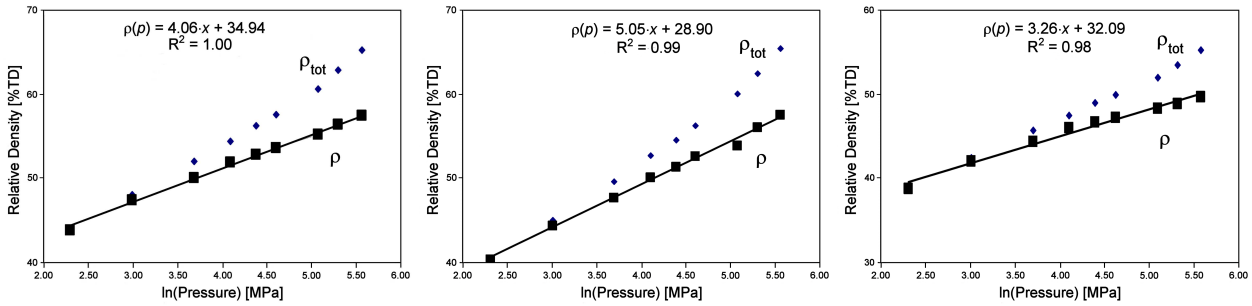

(a) (b) (c)

Figure 7. Compaction curves of: a) MR-01, b) HIM-10 and c) SM-8 granules

Table 3. Spray drying parameters

Sample ID	Compressibility factor	Predicted green density* [%TD]	Measured green density* [%TD]	Difference in predicted and measured green density [%TD]
MR-01	4.06	57.32	57.29	0.052
HIM-10	5.05	57.21	57.47	0.45
SM-8	3.26	49.05	58.13	18.5

*pellet pressed at 260 MPa

retaining the size almost at par with MR-01 alumina. The granule size distribution plays a major role in filling the intra-granular voids between the granules.

It is well known that ceramic granules are not plastic and elastic factors influence the compactability under compaction pressure. When the sample is compacted the strain energy is stored in the compacts. On release of compaction pressure the pellet rebound in the opposite direction. In order to estimate the elastic interaction, a progressive loading under compaction and its periodic unloading was probed. Method of plotting the compaction curves on the basis of one parameter pressing equation is described elsewhere [24]. The compaction curves for MR-01, HIM-10 and SM-8 granules are depicted in Fig. 7. It is observed that the plot of relative density versus compaction pressure of the true compaction curve $\rho(p)$ exhibit the acceptable fit with $R^2 \geq 0.98$. Compaction behaviour is well described by the one parameter logarithmic equation $\rho(p) = 4.06b + 34.94$ for the sample MR-01, $\rho(p) = 5.05b + 28.90$ for the sample HIM-10 and $\rho(p) = 3.26b + 32.09$ for SM-8 granules. Compressibility parameter (b) of the compaction equation provides reliable information on the compaction behaviour of the samples. Predicted and green densities measured by dimensional method are depicted in Table 3.

It is evident that, under identical compaction pressure the compressibility factor and predicted green density based on the instantaneous spring back correlates well in the case of MR-01, HIM-10 and SM-8 samples. Further, the measured density through dimensional method after the compaction cycle is completed and ejection of the compact from the die and the predicted density are within an accuracy of 1% in the case of MR-01 and HIM-10. However, a variation of 19% between the measured and predicted density is observed in the case of the sample SM-8. In present study, the spring back is estimated by instantaneously measuring the ram displacement. Morphology of the granules SM-8 clearly shows that they are hollow in nature, due to ballooning and isolated air pockets are also evident (Fig. 5c). The granule yields under compaction stresses. When the stresses are removed the compact is still within the die wall and probably does not allow easy escape of air which contributes to the observed variation in predicted and measured green density values.

IV. Conclusions

Alumina powders with particle size D_{50} = 0.25, 0.8 and 6 μm were subjected to spray drying under identical conditions and the heat transfer efficiency is found to be maximal for the powder with smallest particle size ($D_{50} = 0.25$ μm), as revealed by the higher outlet temperature and the lowest moisture content of the granules. Morphology, internal structure and size distribution of the granules were found to be a function of particle size. Thus, solid and hollow granules were formed from the alumina powder having particle size $D_{50} = 0.8$ μm (MR-01) and $D_{50} = 0.25$ μm (SM-8), respectively, due to the ballooning effect and dense surface. The granules with distributed voids were obtained from the alumina powder with particle size $D_{50} = 6$ μm (HIM-10). Mechanism for the observed granule structures has been elucidated. Granules size distribution is found to be identical for the samples SM-8 and MR-01 (having particle size $D_{50} = 0.25$ and 0.8 μm, respectively) and distinctly different for the sample HIM-10 (with $D_{50} = 6$ μm),

signifying the effect of primary particle size on granule build up during spray drying. Flow behaviour of the granules was correlated through cohesion index and found to be strong function of their surface morphology. Elastic interaction curves of granules evaluated through progressive loading followed by periodic unloading using uniaxial compaction were plotted. Variation of predicted green densities and actually measured values were also explained based on the granules morphology and internal structure of granules.

References

1. K. Masters, *Spray Drying Handbook*, George Godwin Ltd, UK, 1979.
2. E.H.-J. Kim, X.D. Chen, D. Pearce, "Surface characterization of four industrial spray-dried dairy powders in relation to chemical composition, structure and wetting property", *Colloid Surfaces B: Biointerfaces*, **26** [3] (2002) 197–212.
3. J. Straatsma, G. Van Houwelingen, A.E. Steenbergen, P. De Jong, "Spray drying of food products: 1. Simulation model", *J. Food Eng.*, **42** [2] (1999) 67–72.
4. H. Schubert, "Food particle technology. Part 1: Properties of particles and particulate food systems", *J. Food Eng.*, **6** (1987) 1–32.
5. J. Pisecky, *Handbook of Milk Powder Manufacture*, Niro A/S, Copenhagen, Denmark, 1997.
6. E. Teunou, J.J. Fitzpatrick, E.C. Synnott, "Characterisation of food powder flowability", *J. Food Eng.*, **39** (1999) 31–37.
7. J.L. Ilari, "Flow properties of industrial dairy powders", *Lait*, **82** (2002) 383–399.
8. T.J. Buma, "Free fat in spray-dried whole milk-Cohesion: determination, influence of particle size, moisture content and free fat content", *J. Netherlands Milk Dairy*, **25** (1971) 107–122.
9. C. Vervaet, J.P. Remon, "Continuous granulation in the pharmaceutical industry", *Chem. Eng. Sci.*, **60** [14] (2005) 3949–3957.
10. J. Broadhead, S.K. Edmond Rouan, C.T. Rhodes, "The spray drying of pharmaceuticals", *Drug Develop. Ind. Pharm.*, **18** [11-12] (1992) 1169–1206.
11. A. Carne-Sanchez, I. Imaz, M. Cano-Sarabia, D. Maspoch, "A spray-drying strategy for synthesis of nanoscale metal-organic frameworks and their assembly into hollow superstructures", *Nature Chem.*, **5** (2013) 203–211.
12. D.H. Huntington, "The Influence of the spray drying process on product properties", *Drying Technol.: Int. J.*, **22** [6] (2004) 1261–1287.
13. J.S. Reed, *Principles of Ceramic Processing*, A Wiley-Interscience Publication, New York, 1995.
14. M.N. Rahaman, *Ceramic Processing and Sintering*, Marcel Dekker Inc., New York, 1995.
15. F.F. Lange, "Powder processing science and technology for increased reliability". *J. Am. Ceram. Soc.*, **72** (1989) 3–16.
16. S.J. Glass, K.G. Ewsuk, "Ceramic powder compaction", *MRS Bull.*, **22** [12] (1997) 24–28.
17. D.E. Dobry, D.M. Settell, J.M. Baumann, R.J. Ray, L.J. Graham, R.A. Beyerinck, "A model-based methodology for spray-drying process development", *J. Pharm. Innov.*, **4** (2009) 133–142.
18. A.R. Cooper, L.E. Eaton, "Compaction behavior of several ceramic powders", *J. Am. Ceram. Soc.*, **45** [3] (1962) 97–101.
19. R.A. Thompson, "Mechanics of powder pressing: I, Model for powder densification", *Am. Ceram. Soc. Bull.*, **60** [2] (1981) 237–243.
20. S.J. Lukasiewicz, J.S. Reed, "Character and compaction response of spray–dried agglomerates", *Am. Ceram. Soc. Bull.*, **57** [9] (1978) 798–805.
21. R.A. Youshaw, J.W. Halloran, "Compaction of spray-dried powders", *Am. Ceram. Soc. Bull.*, **61** [2] (1982) 227–230.
22. D.E. Niesz, R.B. Bennett, M. Snyder, "Strength characterization of powder aggregates", *Am. Ceram. Soc. Bull.*, **51** (1972) 677–680.
23. G.L. Messing, C.J. Markhoff, L.G. McCoy, "Characterization of ceramic powder compaction", *Am. Ceram. Soc. Bull.*, **61** [8] (1982) 857–860.
24. R.L.K. Matsumoto, "Generation of powder compaction diagrams", *J. Am. Ceram. Soc.*, **69** [10] (1986) C246–247.
25. O.L. Khasanov, E.S. Dvilis, V.M. Sokolov, "Plotting of compaction curves of ceramic powders on the basis of one-parameter pressing equations", *Ref. Ind. Ceram.*, **42** (2001) 40–44.
26. C.L. Huffine, C.F. Bonilla, "Particle-size effects in the compression of powders", *AICHE J.*, **8** [4] (1962) 490–493.
27. J.A. Hersey, J.E Rees, "The effect of particle size on the consolidation of powders during compaction", pp. 33–41 in *Particle Size Analysis Conference*, 2nd Edition, University of Bradford, UK, 1970.
28. P. Ramavath, M. Swathi, M.B. Suresh, R. Johnson, "Flow properties of spray dried alumina granules using powder flow analysis technique", *Adv. Powd. Technol.*, **24** (2013) 667–673.